ARTICLE   OPEN

Universal, high-fidelity quantum gates based on superadiabatic, geometric phases on a solid-state spin-qubit at room temperature

Felix Kleißler[1], Andrii Lazariev[1] and Silvia Arroyo-Camejo[1]

Geometric phases and holonomies are a promising resource for the realization of high-fidelity quantum operations in noisy devices, due to their intrinsic fault-tolerance against parametric noise. However, for a long time their practical use in quantum computing was limited to proof of principle demonstrations. This was partly due to the need for adiabatic time evolution or the requirement of complex, high-dimensional state spaces and a large number of driving field parameters to achieve universal quantum gates employing holonomies. In 2016 Liang et al. proposed universal, superadiabatic, geometric quantum gates exploiting transitionless quantum driving, thereby offering fast and universal quantum gate performance on a simple two-level system. Here, we report on the experimental implementation of a set of non-commuting single-qubit superadiabatic, geometric quantum gates on the electron spin of the nitrogen-vacancy center in diamond under ambient conditions. This provides a promising and powerful tool for large-scale quantum computing under realistic, noisy experimental conditions.

INTRODUCTION

Currently we reside in an exciting era, in which large-scale circuit-based quantum computers do not exist yet, but their realization appears to become increasingly more feasible. This era of 'Noisy Intermediate-Scale Quantum Computers' (NISQ),[1] offers circuit-based computing platforms with $O(10)$ physical qubits and quantum annealers acting on $O(10^3)$ physical qubits. Despite these impressive achievements in scaling-up the number or qubits, a profound challenge for building viable quantum computers is yet the achievable fidelity of the fundamental quantum gates. Only when fidelity and robustness of the quantum gates are significantly improved, can quantum error correction codes be efficaciously deployed and thus universal large-scale quantum computation will become a reality.

Today, one of the most promising resources for intrinsically fault-tolerant qubit gates are geometric (Abelian) and holonomic (non-Abelian) phases.[2–4] The quantum geometric phase was first shown to arise when a state vector is parallel-transported along a closed loop within a parameter space associated with a non-trivial state space geometry.[5] The value of the geometric phase is determined by global geometric properties of the respective Hilbert space, rather than dynamic parameters. Because parametric noise is characteristic of local nature, geometric phases are prominent to be intrinsically invariant with respect to such small control parameter imperfections.[6] This intrinsic robustness of geometric phases was proposed to deliver a key performance advantage in the context of quantum computation. However, a general resilience of geometric phase-based quantum gates against decoherence effects (in open quantum system) has not been demonstrated theoretically or experimentally to the best of our knowledge. Zanardi and Rasetti were pioneers to propose quantum gate evolution based on holonomies, i.e., non-Abelian geometric phases.[7,8] However, the quantum systems coherence time in combination with adiabatic system evolutions limited geometric quantum gates to proof-of-principle demonstrations without much practical relevance.[9]

Only recently the generalization towards non-Abelian, non-adiabatic holonomic quantum gates (HQG) broke this limitation by nonadiabatically transporting a computational subspace in a higher-dimensional Hilbert space.[10] To this end, the holonomy arises from the rotation of a complex vector (represented by a Rabi oscillation between the bright and excited states of the dressed three-level system) around a static, complex vector given by the dark state. Experimental realizations[11–13] of this HQG concept achieved high-fidelity quantum gate performance exceeding the threshold required for the implementation of quantum error correction protocols.[14,15] Because a holonomy can only arise in a more than two-dimensional Hilbert space the implementation of HQG requires higher-dimensional quantum systems with at least two well controlled driving fields (for examples see refs. [16–21]).

In contrast, non-adiabatic geometric phases[22–24] allow for quantum computation in a two-dimensional computational space equivalent to the systems Hilbert space at the cost of time-dependent driving fields. Until now, the realization of the latter has been pending. Here, we report the first realization of a recently proposed single-qubit superadiabatic geometric quantum gate (SAGQG) scheme[25] which exploits the concept of transitionless quantum driving (TQD)[26] to realize adiabatic state evolution in finite time (i.e., a significantly shorter time frame than conventionally suggested by the adiabatic theorem). The gate operations are generated by controlling a single time-dependent driving field keeping the experimental resources minimal, while

[1]Department of NanoBiophotonics, Max Planck Institute for Biophysical Chemistry, Am Faßberg 11, 37077 Göttingen, Germany
Correspondence: Felix Kleißler (fkleiss@mpibpc.mpg.de) or Silvia Arroyo-Camejo (sarroyo@mpibpc.mpg.de)

npj
Universal, high-fidelity quantum gates based on superadiabatic…
F Kleißler et al.

2

combining the advantages of geometric and superadiabatic evolutions.

Experiments are performed utilizing the electron spin dedicated to the nitrogen-vacancy (NV) center in diamond, a promising candidate for the implementation of a scalable quantum registers. Dynamic single-qubit[27] and multi-qubit[28] gates as well as non-adiabatic non-Abelian geometric single-qubit gates[13] have demonstrated its significance for quantum information applications, even at room-temperature. Moreover, the use of optimized samples eliminates/supresses the noise environment as source of error and high fidelity quantum computation can be obtained by choosing quantum operations insensitive to control parameter imperfections.

RESULTS

Superadiabatic geometric quantum gates

The SAGQG proposal[25] builds upon the concept of the Aharonov-Anandan type non-adiabatic geometric phase.[29] For the Aharonov-Anandan phase to be solely of geometric nature, in the total phase

$$\Phi = -\int_0^T \langle\psi(t)|H(t)|\psi(t)\rangle dt + \int_0^T \langle\tilde{\psi}(t)|i(\partial/\partial t)\tilde{\psi}(t)\rangle dt \quad (1)$$

the first, dynamic-phase term must vanish (here $|\tilde{\psi}(t)\rangle$ is the reference section state on the projective Hilbert space $\mathcal{P}$[30]). This can be achieved by driving the state vector with a driving field that is applied perpendicularly to the state vector at all times. Under this condition driving the state vector on the Bloch sphere, the solid angle $\tilde{\Omega}$ enclosed by the Bloch vector trajectory determines the acquired geometric phase $\gamma = \Phi = \tilde{\Omega}/2$ (Fig. 1a).

The Aharonov-Anandan phase is restricted to generate U(1) phase shift gates. The total Hamiltonian of the SAGQG is constructed employing the technique of transitionless driving[26] where a reverse engineered correction Hamiltonian compensates for undesired transitions between the basis states. This way the effective superadiabatic Hamiltonian drives the instantaneous eigenstates exactly such that non-adiabatic correction terms are cancelled and the evolution of dynamic phases is fully suppressed, even within the fast driving regime.

Considering a two-level system with a time-dependent single driving field, our original Hamiltonian $H_0(t)$ has the following form in the co-rotating reference frame of the external driving field

$$H_0(t) = \frac{\hbar}{2}\begin{pmatrix} \Delta(t) + \dot{\Delta}(t)t & \Omega_R(t)e^{-i\varphi} \\ \Omega_R(t)e^{i\varphi} & -(\Delta(t) + \dot{\Delta}(t)t) \end{pmatrix}, \quad (2)$$

where the driving field is applied with a detuning $\Delta(t) = \omega_0 - \omega_D(t)$, with ω_0 the qubit resonance frequency and $\omega_D(t)$ the driving

field frequency, phase φ, and Rabi frequency $\Omega_R(t)$. The non-standard form of the Hamiltonian in Eq. (2) in the rotating frame of the driving field arises from its time-dependent detuning (see Supplementary Information for details on the derivation of Eq. (2)). Exploiting the concept of TQD[26] and deriving a suitable correction Hamiltonian H_c Liang et al.[25] propose the superadiabatic Hamiltonian

$$H_S(t) = H_0 + H_c = \frac{\hbar}{2}\begin{pmatrix} \Delta(t) + \dot{\Delta}(t)t & \Omega_S(t)e^{-i[\varphi+\phi_S(t)]} \\ \Omega_S(t)e^{i[\varphi+\phi_S(t)]} & -(\Delta(t) + \dot{\Delta}(t)t) \end{pmatrix}, \quad (3)$$

where $\Omega_S(t) = \sqrt{\Omega_R(t)^2 + \Omega_C(t)^2}$ is the superadiabatic Rabi frequency, and $\varphi_S(t) = \arctan[\Omega_C(t)/\Omega_R(t)]$ is the superadiabatic phase. The corrected Rabi frequency is $\Omega_C(t) = [\dot{\Omega}_R(t)(\Delta(t) + \dot{\Delta}(t)t) - \Omega_R(t)\partial_t(\Delta(t) + \dot{\Delta}(t)t)]/\Omega^2$, where the generalized Rabi frequency is introduced as $\Omega = \sqrt{\Omega_R(t)^2 + (\Delta(t) + \dot{\Delta}(t)t)^2}$. The instantaneous eigenstates of the original Hamiltonian $H_0(t)$ are $|\lambda_\pm(t)\rangle$. (The explicit expression of the superadiabatic Rabi frequency $\Omega_S(t)$, detuning $\Delta_S(t) = \Delta(t) + \dot{\Delta}(t)t$ and phase $\varphi(t)$ are given in the 'Methods' section.)

In order to realize universal quantum computation the SAGQG applies a strategy previously developed by Zhu and Wang[23,31] which is based on choosing a pair of orthogonal states $|\lambda_\pm(t)\rangle$ undergoing a cyclic evolution: $|\lambda_\pm(T)\rangle = \exp[i\phi_\pm]|\lambda_\pm(0)\rangle$. Over the full length of the SAGQG transformation the dynamic phase is designed to cancel such that the system evolution becomes fully geometric $U(T,0)|\lambda_\pm(0)\rangle = \exp[\pm i\gamma]|\lambda_\pm(0)\rangle$ where the evolution operator $U(T, 0)$ imprints only a U(1) phase factor on each of the eigenstates $|\lambda_\pm(0)\rangle$. Wang and Zhu ingeniously identified that these trivial phase factors on the $|\lambda_\pm(0)\rangle$ nevertheless translate to a non-Abelian transformation on the computational states in the co-rotating frame. Thus, even though the SAGQG is not based on a non-Abelian holonomy, in virtue of the elaborate basis transformation between the cyclic states and the computational states the U(1) geometric-phase factors convert to a non-Abelian, geometric transformation of the computational states allowing for universal quantum computation.

Bloch sphere trajectory

The SAGQG state evolution is based on a sequence of four trajectory segments of time duration τ, leading to a total gate length of $t_{Gate} = 4\tau$ (see Methods section for details). We investigate and visualize the quantum gate Bloch sphere trajectory of a qubit initialized into the $|0\rangle$ state in a stroboscopic manner by applying projective readout pulses at times t_m. As two representative gates we realize the Pauli-Z (Fig. 2a, b) and the Pauli-X (Fig. 2c, d) gate. The measured Bloch vector trajectories (dots) are in very good agreement with the numerically calculated trajectories (solid lines). Rotations around the y-axis (Pauli-Y gate) can be realized by setting $\varphi = \pi/2$ for the original Hamiltonian $H_0(t)$. In the realization of the Pauli-Z gate, the non-adiabatically obtained original trajectory is observed (compare Fig. 1a), since the input eigen state $|0\rangle$ is equivalent to the Hamiltonians instantaneous eigenstate $|\lambda_\pm(0)\rangle$ at $t = 0$. The particular shape of the trajectory in Fig. 2c, d illustrates that the geometric phase is obtained utilizing a sophisticated parameter time-dependence.

Generalization to geometric gate with arbitrary phase value

So far we demonstrated that rotations by $\gamma = \pi/2$ around the x and z-axis can be fulfilled with high fidelity by performing super-adiabatic geometric quantum computation. In addition, by varying the opening angle of the "orange slice" trajectory an arbitrary geometric phase γ can be acquired. Utilizing the states $|0\rangle$, $1/\sqrt{2}(|0\rangle - |1\rangle)$ and $1/\sqrt{2}(|0\rangle + i|1\rangle)$ we demonstrate the rotation for different geometric phases γ (see Fig. 2e–k). In order to
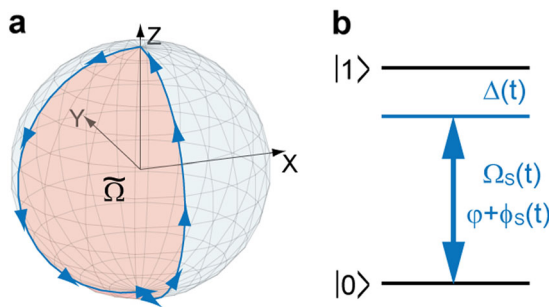

Fig. 1 Superadiabtic geometric quantum gate concept. **a** Anticipated "orange slice" Bloch sphere trajectory (blue) enclosing the solid angle $\tilde{\Omega} = 2\gamma$ (red). **b** Two-level system and microwave field parameter (detuning $\Delta(t)$, Rabi frequency $\Omega_S(t)$ and phase $\varphi + \phi_S(t)$) utilized for the realization of superadiabatic geometric quantum computation

Universal, high-fidelity quantum gates based on superadiabatic…
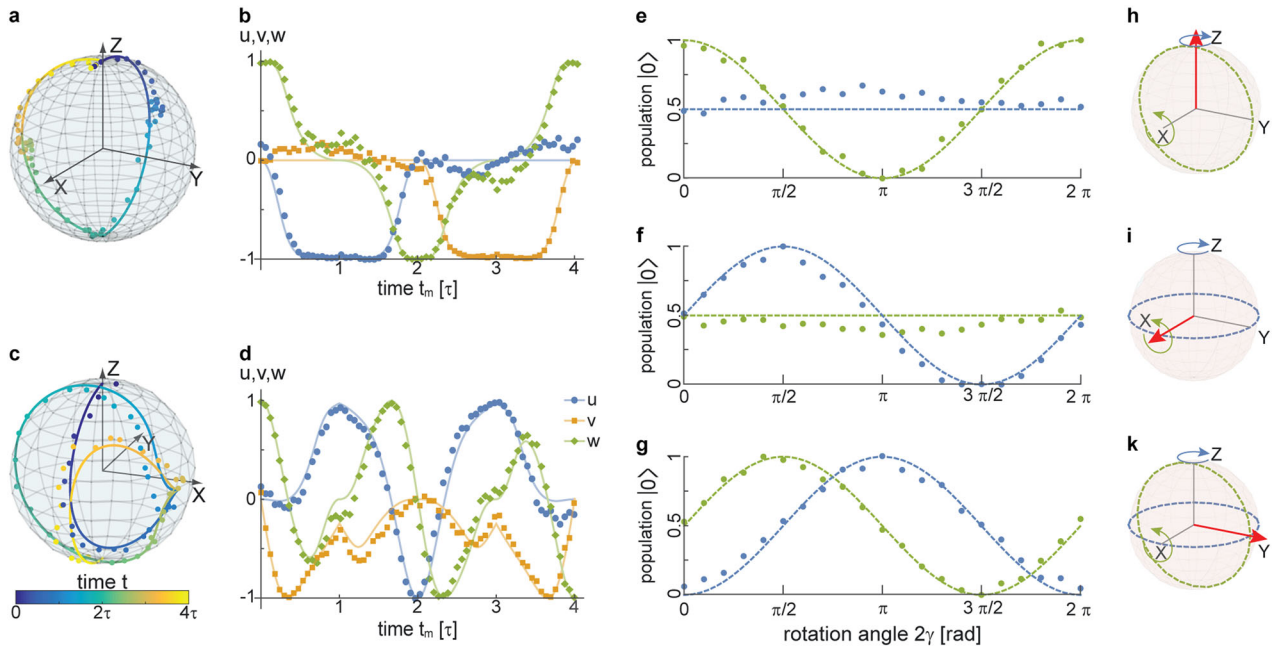F Kleißler et al.

npj

3

Fig. 2 Superadiabatic geometric gate realization: **a** Simulated and reconstructed Bloch sphere trajectory of the superadiabatic geometric Pauli-Z gate in the driving field frame for a spin initialized into the $|0\rangle$ state. **b** Bloch vector components $u(t) = \rho_{10}(t) + \rho_{01}(t)$ (blue), $v(t) = i(\rho_{01}(t) - \rho_{10}(t))$ (orange) and $w(t) = \rho_{00}(t) - \rho_{11}(t)$ (green), where $\rho(t)$ is the density matrix representation of the instantaneous state, of the trajectory presented in **a** versus the gate time in multiples of τ. Solid lines represent numerically calculated trajectories and dots indicate measured values. Analogously **c** and **d** follow for the realized Pauli-X gate. **e–g** Measured population of the $|0\rangle$ state for a spin initialized into the states **e** $|0\rangle$, **f** $1/\sqrt{2}(|0\rangle - |1\rangle)$ and **g** $1/\sqrt{2}(|0\rangle + i|1\rangle)$ in dependence on γ for superadiabatic rotations around the x (green) and z-axis (blue). Dashed lines represent the expected values. Bloch spheres **h**, **i**, **k** indicate the initialized state (red arrow)

visualize the phase gate we map the acquired phase into a population by application of a projective $\pi/2$-pulse around the $\bar{y}$-axis. Hence, we show that the SAGQG concept additionally allows for the generation of an arbitrary phase shift gate. Collectively with the former we thus provide a universal set of single-qubit geometric quantum gates.

Fidelity assessment and fault-tolerance
Quantification of the performance of the superadiabatic geometric gates is obtained via standard quantum process tomography (QPT)[32] measurements, which allow to reconstruct the full experimental quantum process matrix χ_{exp} and therefore to determine the quantum gate fidelity $F = \text{Tr}(\chi_{exp}\chi_0)$,[33] where χ_0 is the theoretically anticipated process matrix (for details on the experimental QPT procedure see Supplementary Information and ref. [13]). Due to their dynamic nature and finite time duration the QPT pulses are susceptible to errors and we obtain the corrected quantum gate fidelity value $\tilde{F} = F/F_{ID}$ by normalization with the fidelity of the identity operation. We determine the experimental gate fidelities of the SAGQG to be $\tilde{F}_x^{SAGQG} = 0.994^{+0.026}_{-0.031}$ and $\tilde{F}_z^{SAGQG} = 0.995^{+0.021}_{-0.024}$ for Pauli-X and Pauli-Z operations, respectively. Additionally, the Hadamard gate is realized by a rotation of $\pi/2$ around the y-axis ($R_y(\pi/2)$) and a subsequent rotation by π around the z-axis ($R_z(\pi)$), resulting in an experimental fidelity of $\tilde{F}_H^{SAGQG} = 0.992^{+0.022}_{-0.029}$. These values clearly exceed the necessary fidelity threshold on the order of $1 - 10^{-2}$ for the implementation of state-of-the-art error correction codes based on, e.g., surface codes.[34,35] The SAGQG concept thus qualifies as a promising candidate for the implementation of scalable quantum computing.

Besides the fidelity of the individual, logical gates, we additionally assess the average error probability over the set of universal gates employing randomized benchmarking.[36] Based on the application of randomly assembled sequences of a set of logical gates, randomized benchmarking allows for a good estimation of the error scaling given a long sequence of quantum gates, as relevant for viable applications in longer quantum algorithms. Figure 3a presents the average fidelity as a function of the number of computational gates l. For the SAGQG we obtain an average probability of error per gate of $\varepsilon_g^{SAGQG} = 0.0013(3)$, whereas an identical analysis for a set of dynamic quantum gates represented by π and $\pi/2$-pulses reveals an average probability of error of $\varepsilon_g^{dynamic} = 0.023(8)$, i.e., the geometric-phase based SAGQG performs one order of magnitude better than its dynamic-phase based standard gate (see Supplementary Information for details). Our results suggest that the SAGQG is significantly more resilient with respect to the type of noise and parameter imperfections present in our experimental system than the standard realization of dynamic phase-based quantum gates. Since the longest sequence duration (in total 99 gates) is much shorter than the longitudinal relaxation time ($T_{seq} \approx 32\,\mu s << T_1 \approx 14\,ms$), decoherence effects are expected to be negligible and parametric noise is assumed to be the main source of error. Our experimental findings demonstrate the intrinsic robustness of non-adiabatic geometric phase-based quantum gates with respect to certain, experimentally very relevant types of parametric noise. These experimental findings of a non-adiabatic geometric quantum gate (Table 1) are in accordance with theoretical predictions of robustness in the distinct, but related adiabatic geometric gates.[6,8,37–39] This joint robustness trait can be attributed to the fact that both adiabatic and non-adiabatic geometric phases and holonomies are global features, which are intrinsically robust with respect to locally occurring parameter imperfections and noise leaving the state-space area enclosed by the trajectory on the respective projective space invariant.

In the following we examine the fidelity performance of the SAGQG with respect to variations in the gate evolution time. This is important for two reasons: (1) In order to most efficiently exploit the coherence time of the qubit, we need to investigate the
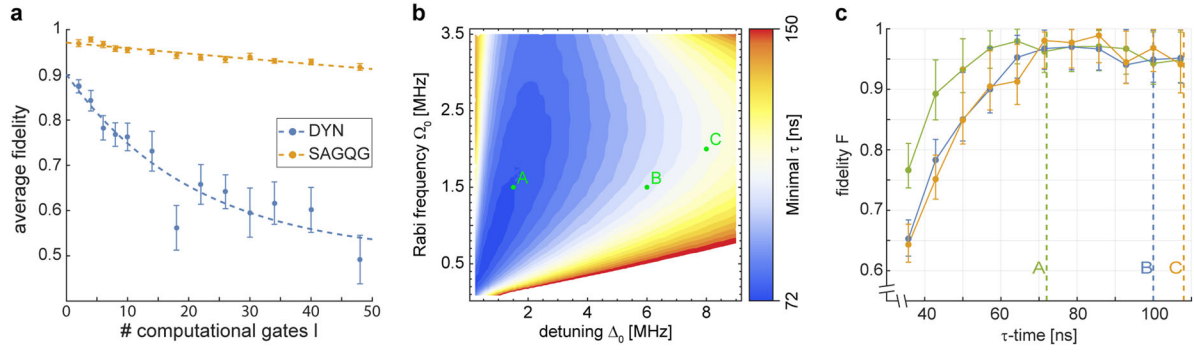
npj
Universal, high-fidelity quantum gates based on superadiabatic…
F Kleißler et al.

4

Fig. 3 Robustness analysis: **a** The randomized benchmarking analysis reveals the decay of the average fidelity in dependence of the number of computational gates l for a set of SAGQG (orange) and a set of dynamic quantum gates (blue). The average probability of error per gate are $\varepsilon_g^{SAGQG} = 0.0013(3)$ and $\varepsilon_g^{Dynamic} = 0.023(8)$, respectively. Error bars represent the standard error of the mean. **b** Minimal value of τ in dependence on the free parameter Ω_0 and Δ_0 for a system with maximal Rabi frequency $\Omega_{max} = 7$ MHz. **c** Measured quantum gate fidelity F as a function of τ for three free parameter combinations indicated in **b** by A, B and C. Solid lines are a guide to the eye. Vertical dashed lines represent the numerically calculated minimal τ value fulfilling $\Omega_S(t, \tau, \Omega_0, \Delta_0) \leq \Omega_{max}$

Table 1. Experimentally obtained corrected quantum gate fidelities $\tilde{F}$ and average gate error ε_g of the single-qubit SAGQGs

$\tilde{F}_X$	$\tilde{F}_Z$	$\tilde{F}_H$	ε_g
$0.994^{+0.026}_{-0.031}$	$0.995^{+0.021}_{-0.024}$	$0.992^{+0.022}_{-0.029}$	$0.0013(3)$

theoretical velocity limits and experimental performance of the SAGQG and aim for fast quantum gate performance. (2) We experimentally examine the intrinsical robustness of the SAGQG with respect to experimental parameter imperfections. In particular we analyse the SAGQG performance outside its optimal parameter specifications. The latter is particularly relevant for the common experimental case where the Rabi frequency (for practical reasons) obeys a maximum bound $\max_t(\Omega_S(t, \Omega_0, \Delta_0)) \leq \Omega_{max}$ (for parameter dependences see 'Methods' section). Given such a practical maximum bound Ω_{max} for the experimentally achievable Rabi frequency, in Fig. 3b we show a contour plot of the numerically determined minimal τ-value, denoted $\tau_{min}(\Omega_0, \Delta_0)$, fulfilling the necessary criterion $\max_t(\Omega_S(t, \Omega_0, \Delta_0)) \leq \Omega_{max}$. We like to stress again, the $\tau_{min}(\Omega_0, \Delta_0)$ limit is not given by theoretical constraints related to the state evolution (e.g., adiabaticity), but it is merely defined by the experimentally achievable Rabi strength Ω_{max}. The smallest, experimentally feasible τ-value is equivalent to $1/(2\Omega_{max})$ corresponding to the length of a π-pulse t_π, ultimately limiting the SAGQG length to $t_{Gate} \geq 2/\Omega_{max} = 4t_\pi$. For our experimental conditions the minimal gate length $t_{Gate} = 4\tau_\pi$ corresponds to $t_{Gate} = 284$ ns. If τ were chosen smaller than τ_{min} this would require $\max_t(\Omega_S(t, \Omega_0, \Delta_0))$ to exceed Ω_{max} which— given experimental limitations on Ω_{max}—cannot be fulfilled by any experimental parameter set. Forcing $\tau < \tau_{min}$ experimentally leads to a marked mismatch between required and actual value of the driving field strength $\Omega_S(t)$, i.e., an inconsistent, erroneous driving field parameter set.

For an experimental robustness analysis of the SAGQG we explicitly vary the gate time parameter τ within a non-optimal range of τ reaching from $0.5 \cdot t_\pi$ to $1.5 \cdot t_\pi$ (whereas the theoretical $\min_{\Omega_0, \Delta_0}(\tau_{min}) = t_\pi$) for three sets of parameters A, B, and C ($\Omega_0 = \{1, 1.5, 2\}$ MHz and $\Delta_0 = \{1.5, 6, 8\}$ MHz). The $\min_{\Omega_0, \Delta_0}(\tau_{min})$ value for each parameter set is marked in Fig. 3c as a vertical, dashed line of matching colors, respectively. Figure 3c shows the extracted quantum gate fidelity F of the Pauli-X gate in dependence of τ. We observe that even for τ smaller than the calculated threshold τ_{min} the quantum gate fidelity F remains close to one. Only for $\tau < t_\pi \approx 71$ ns is the fidelity dropping. These results proof the tolerance of the SAGQG to perform stably over a large range of timing parameter variations and give evidence for the intrinsic robustness of the SAGQG against timing imprecision and concomitant mismatches in the driving field strength.

DISCUSSION

In this work we demonstrated the experimental realization of the recently proposed universal set of single-qubit SAGQGs, utilizing the NV center electron spin in diamond at room temperature. Our experimental demonstration exhibits fast and high-fidelity qubit gate performance while requiring only a minimalistic qubit and control system for its realization, if compared to schemes based on holonomic qubit gates reaching similar high-fidelity performance. The realization within a two-level system sets comparatively low requirements on the experimental apparatus and the single driving field reduces the number of control parameters significantly. We explicitly investigated and confirmed the tolerance of this gate type with respect to errors in the gate time and experimentally verified its robustness.

An extension of the SAGQG concept to a two-qubit controlled-NOT and controlled-PHASE has been proposed[25] and would, together with the single-qubit set presented here, provide a universal set of SAGQGs. Beyond the demonstration in this work performed on an NV center spin qubit, this single-qubit gate technique is directly translatable to other promising experimental qubit systems, like, e.g., atomic, ion, transmon or flux qubits. Beyond quantum computing, the SAGQG concept presented here could be employed as a universal, high-fidelity building block for other novel quantum technologies being fundamentally based on quantum operations, like quantum communication or qubit-assisted nanosensing applications.

METHODS

Original Hamiltonian

In the following the driving field parameter for the realization of superadiabatic phase gate according to Liang et al.[25] are listed. The Rabi frequency used to yield $\Omega_S(t)$ reads

$$\Omega_R(t) = \begin{cases} \Omega_0 \left[1 - \cos\frac{\pi t}{\tau}\right], & 0 \leq t < \tau \\ \Omega_0 \left[1 + \cos\frac{\pi(t-\tau)}{\tau}\right], & \tau \leq t < 2\tau \\ \Omega_0 \left[1 - \cos\frac{\pi(t-2\tau)}{\tau}\right], & 2\tau \leq t < 3\tau \\ \Omega_0 \left[1 + \cos\frac{\pi(t-3\tau)}{\tau}\right], & 3\tau \leq t \leq 4\tau \end{cases} \quad (4)$$

Universal, high-fidelity quantum gates based on superadiabatic…
F Kleißler et al.

np

5

To obtain the experimentally relevant detuning $\Delta(t)$ of the driving field the following differential equation needs to be solved for:

$$\Delta_s(t) = \Delta(t) + \dot{\Delta}(t)t = \begin{cases} \Delta_0 \left[\cos\frac{\pi t}{\tau} + 1\right], & 0 \leq t < \tau \\ \Delta_0 \left[\cos\frac{\pi(t-\tau)}{\tau} - 1\right], & \tau \leq t < 2\tau \\ \Delta_0 \left[\cos\frac{\pi(t-2\tau)}{\tau} + 1\right], & 2\tau \leq t < 3\tau \\ \Delta_0 \left[\cos\frac{\pi(t-3\tau)}{\tau} - 1\right], & 3\tau \leq t \leq 4\tau \end{cases} \quad (5)$$

The value of the acquired geometric phase $\gamma = \pi - (\tilde{\varphi}_1 - \tilde{\varphi}_2)$ is defined by constant phases $\tilde{\varphi}_1$ and $\tilde{\varphi}_2$ added to the driving field phase

$$\varphi + \phi_s(t) = \begin{cases} \tilde{\varphi}_1 + \phi_s(t), & 0 \leq t < 2\tau \\ \tilde{\varphi}_2 + \phi_s(t), & 2\tau \leq t \leq 4\tau \end{cases}. \quad (6)$$

For the realization of the Pauli-Z gate presented here we set $\tilde{\varphi}_1 = 0$ and $\tilde{\varphi}_2 = \pi/2$ resulting in the wanted phase value of $\gamma = \pi/2$. The driving field parameter for the realization of a spin-flip gate follow in a similar manner and are shown in the supplementary material explicitly.

NV center in diamond

The NV center consists of a substitutional nitrogen atom and an adjacent vacant lattice site in the carbon diamond lattice. A spin-one system is associated with the negatively charged NV species, which can be efficiently initialized[40] and readout[41] by optical means. The triplet ground state features a zero field splitting of $D \approx 2\pi \times 2.87$ GHz between the $m_s = 0$ and $m_s = -1$, $m_s = +1$ states. Aligning an external magnetic field of $|B| \approx 400$ G along the NV center axis enables dynamic nuclear polarization of the nitrogen nuclear spin[42,43] and sets the triplet transition frequencies to $m_s = 0 \leftrightarrow m_s = -1 (\omega_{0-} \approx 2\pi \times 1.73$ GHz$)$ and $m_s = 0 \leftrightarrow m_s = +1 (\omega_{0+} \approx 2\pi \times 4.01$ GHz$)$. Both transitions can be manipulated coherently by applying microwave fields at frequencies $\omega_- = \omega_{0-} + \delta_-$ and $\omega_+ = \omega_{0+} + \delta_+$, where $\delta_\pm$ is the detuning from the resonance. For our experiments we employ the two-level system comprised of the $m_s = 0$ and $m_s = -1$ states. We define $m_s = 0$ and $m_s = -1$ as the logic states $|0\rangle$ and $|1\rangle$, respectively.

Experimental realization

A custom-made confocal microscope equipped with a 546 nm cw laser serves for optical initialization of the NV spin qubit and facilitates optical readout of the final spin states from the NV spin's emitted fluorescence intensity. Coherent microwave manipulation is conducted by means of an arbitrary waveform generator (AWG) that can be programmed at a high sampling rate of 25 GSamples/s as needed. While the Rabi frequency and detuning of the applied MW field needed to follow specific time-dependences, maximum values were $\Omega_s = 7$ MHz and $\Delta_s = 2$ MHz.

The employed NV center was generated in an isotopically pure diamond from Element 6 (99.999% ^{12}C abundance) as grown diamond substrate, by ^{14}N ion implantation at around 10 MeV, leading to the formation of NV center in a depth of around 3.7 μm below the diamond surface after annealing. We determine a longitudinal relaxation time of $T_1 = (13.7 \pm 2.2)$ ms and a spin-dephasing time of $T_2^* = (4.25 \pm 0.27)$ μs. At a magnetic field of ≈ 402 G aligned along the NV center axis we obtain a nuclear polarization of 0.94 ± 0.05 G into the $m_I = +1$ hyperfine state.

AUTHOR CONTRIBUTIONS

F.K., S.A.-C., and A.L. performed and evaluated the experiments. S.A.-C. and F.K. performed analytical and numerical calculations and data analysis. A.L. and S.A.-C. designed and programmed the experiment control software. F.K. and S.A.-C. wrote the manuscript. S.A.-C. conceived and supervised the project.

REFERENCES

1. J. Preskill. Quantum Computing in the NISQ era and beyond. *ArXiv e-prints*, January 2018.
2. Filipp, S. et al. Experimental demonstration of the stability of berry's phase for a spin-1/2 particle. *Phys. Rev. Lett.* **102**, 030404 (2009).
3. Johansson, M. et al. Robustness of nonadiabatic holonomic gates. *Phys. Rev. A* **86**, 062322 (2012).
4. Berger, S. et al. Exploring the effect of noise on the berry phase. *Phys. Rev. A* **87**, 060303 (2013).
5. Berry, M. V. Quantal phase factors accompanying adiabatic changes. *Proc. R. Soc. Lond., Ser. A* **392**, 45–57 (1984).
6. De Chiara, G. & Palma, G. M. Berry phase for a spin 1/2 particle in a classical fluctuating field. *Phys. Rev. Lett.* **91**, 090404 (2003).
7. Wilczek, F. & Zee, A. Appearance of gauge structure in simple dynamical systems. *Phys. Rev. Lett.* **52**, 2111–2114 (1984).
8. Zanardi, P. & Rasetti, M. Holonomic quantum computation. *Phys. Lett. A* **264**, 94–99 (1999).
9. Jones, J. A., Vedral, V., Ekert, A. & Castagnoli, G. Geometric quantum computation using nuclear magnetic resonance. *Nature* **403**, 869–871 (2000).
10. Sjöqvist, E. et al. Non-adiabatic holonomic quantum computation. *New J. Phys.* **14**, 103035 (2012).
11. Abdumalikov, A. A. Jr. et al. Experimental realization of non-abelian non-adiabatic geometric gates. *Nature* **496**, 482–485 (2013).
12. Feng, G., Xu, G. & Long, G. Experimental realization of nonadiabatic holonomic quantum computation. *Phys. Rev. Lett.* **110**, 190501 (2013).
13. Arroyo-Camejo, S., Lazariev, A., Hell, S. W. & Balasubramanian, G. Room temperature high-fidelity holonomic single-qubit gate on a solid state spin. *Nat. Commun.* **5**, 4870 (2014).
14. Shor, P. W. Scheme for reducing decoherence in quantum computer memory. *Phys. Rev. A* **52**, R2493–R2496 (1995).
15. Knill, E. Quantum computing with realistically noisy devices. *Nature* **434**, 39–44 (2005).
16. Unanyan, R. G., Shore, B. W. & Bergmann, K. Laser-driven population transfer in four-level atoms: Consequences of non-abelian geometrical adiabatic phase factors. *Phys. Rev. A* **59**, 2910–2919 (1999).
17. Duan, L.-M., Cirac, J. I. & Zoller, P. Geometric manipulation of trapped ions for quantum computation. *Science* **292**, 1695–1697 (2001).
18. Xu, G. F., Zhang, J., Tong, D. M., Sjöqvist, E. & Kwek, L. C. Nonadiabatic holonomic quantum computation in decoherence-free subspaces. *Phys. Rev. Lett.* **109**, 170501 (2012).
19. Liang, Z.-T., Du, Y.-X., Huang, W., Xue, Z.-Y. & Yan, H. Nonadiabatic holonomic quantum computation in decoherence-free subspaces with trapped ions. *Phys. Rev. A* **89**, 062312 (2014).
20. Zhang, J., Kyaw, T. H., Tong, D. M., Sjöqvist, E. & Kwek, L. C. Fast non-abelian geometric gates via transitionless quantum driving. *Sci. Rep.* **5**, 18414 (2015).
21. Santos, A. C. & Sarandy, M. S. Superadiabatic controlled evolutions and universal quantum computation. *Sci. Rep.* **5**, 15775 (2015).
22. Wang, X.-B. & Keiji, M. Nonadiabatic conditional geometric phase shift with nmr. *Phys. Rev. Lett.* **87**, 097901 (2001).
23. Zhu, S.-L. & Wang, Z. D. Implementation of universal quantum gates based on nonadiabatic geometric phases. *Phys. Rev. Lett.* **89**, 097902 (2002).
24. Zhu, S. L., Wang, Z. D. & Zanardi, P. Geometric quantum computation and multiqubit entanglement with superconducting qubits inside a cavity. *Phys. Rev. Lett.* **94**, 100502 (2005).
25. Liang, Zhen-Tao et al. Proposal for implementing universal superadiabatic geometric quantum gates in nitrogen-vacancy centers. *Phys. Rev. A* **93**, 040305(R) (2016).
26. Berry, M. V. Transitionless quantum driving. *J. Phys. A: Math.* **42**, 365303 (2009).
27. Kennedy, T. A. et al. Single-qubit operations with the nitrogen-vacancy center in diamond. *Phys. Stat. Sol. (b)* **233**, 416–426 (2002).

6

28. Dolde, F. et al. Room-temperature entanglement between single defect spins in diamond. *Nat. Phys.* **9**, 139–143 (2013).

29. Aharonov, Y. & Anandan, J. Phase change during a cyclic quantum evolution. *Phys. Rev. Lett.* **58**, 1593–1596 (1987).

30. Pati, A.-K. Gauge-invariant reference section and geometric phase. *J. Phys. A. Math. Gen.* **28**, 2087 (1995).

31. Shi-Liang Zhu & Wang, Z. D. Universal quantum gates based on a pair of orthogonal cyclic states: application to nmr systems. *Phys. Rev. A.* **67**, 022319 (2003). Feb.

32. O'Brien, J. L. et al. Quantum process tomography of a controlled-not gate. *Phys. Rev. Lett.* **93**, 080502 (2004).

33. Nielsen, M. A. & Chuang, I. L. *Quantum Computation and Quantum Information.* (Cambridge University Press, Cambridge, 2005).

34. Kitaev, A. Y. Quantum computations: algorithms and error correction. *Russ. Math. Surv.* **52**, 1191 (1997).

35. Fowler, A. G., Mariantoni, M., Martinis, J. M. & Cleland, A. N. Surface codes: towards practical large-scale quantum computation. *Phys. Rev. A* **86**, 032324 (2012).

36. Knill, E. et al. Randomized benchmarking of quantum gates. *Phys. Rev. A* **77**, 012307 (2008).

37. Solinas, P., Zanardi, P. & Zanghi, N. Robustness of non-abelian holonomic quantum gates against parametric noise. *Phys. Rev. A* **70**, 042316 (2004).

38. Zhu, S.-L. & Zanardi, P. Geometric quantum gates that are robust against stochastic control errors. *Phys. Rev. A* **72**, 020301 (2005).

39. Solinas, P., Sassetti, M., Truini, P. & Zanghi, N. On the stability of quantum holonomic gates. *New J. Phys.* **14**, 093006 (2012).

40. Gaebel, T. et al. Room-temperature coherent coupling of single spins in diamond. *Nature* **2**, 408–413 (2006).

41. Gurudev Dutt, M. V. et al. Quantum register based on individual electronic and nuclear spin qubits in diamond. *Science* **316**, 1312–1316 (2007).

42. Smeltzer, B., McIntyre, J. & Childress, L. Robust control of individual nuclear spins in diamond. *Phys. Rev. A* **80**, 050302 (2009).

43. Jacques, V. et al. Dynamic polarization of single nuclear spins by optical pumping of nitrogen-vacancy color centers in diamond at room temperature. *Phys. Rev. Lett.* **102**, 057403 (2009).